Nuclear Materials and Energy 19 (2019) 262–266

Contents lists available at ScienceDirect

Nuclear Materials and Energy

journal homepage: www.elsevier.com/locate/nme

Micro- and macro- elastic properties of tungsten fiber-reinforced tungsten composites probed by nano-indentation and laser ultrasonics

H.T. Lee[a,*], S. Ando[a], J.W. Coenen[b], Y. Mao[b], R. Kasada[c], J. Riesch[d], Y. Ueda[a]

[a] Graduate School of Engineering, Osaka University, Suita, Osaka 565-0871, Japan
[b] Forschungszentrum Jülich GmbH, Institut für Energie- und Klimaforschung – Plasmaphysik, Partner of the Trilateral Euregio Cluster (TEC), Jülich 52425, Germany
[c] Institute of Materials Research, Tohoku University, Aoba-ku, Sendai 980-8577, Japan
[d] Max-Planck-Institut für Plasmaphysik, Garching 85748, Germany

A B S T R A C T

The elastic properties of tungsten fiber-reinforced tungsten composites (W_f/W) were characterized on the micro- and macro- scale by combined nano-indentation and laser ultrasonic measurements, respectively. W_f/W composite materials are currently being developed as advanced tungsten (W) plasma facing materials for fusion devices. They possess pseudo-ductility and can overcome some of the limitations caused by the inherent brittleness of pure-W at lower temperatures. The Young's modulus was determined by nano-indentation hardness measurements of the W-matrix and W-fibers separately. The values were combined by simple rule of mixture, and compared to bulk values obtained from laser ultrasonics measurements. The results show that the simple rule of mixtures is valid up to 50% fiber volume fractions.

1. Introduction

Elastic mechanical properties of divertor plasma facing components in fusion devices are important because they determine the thermal stresses arising from cyclical power loads. Such thermal stresses can lead to surface cracking from fatigue, resulting in new leading edges. For the case of tungsten (W) divertor components such leading edges can melt, decreasing the lifetime and increasing the potential for component failure. To improve the performance, tungsten fiber-reinforced tungsten composites (W_f/W) are presently being developed as advanced tungsten plasma facing materials. They possess pseudo-ductility and can therefore overcome some of the limitations caused by the inherent brittleness of pure-W [1]. For composites, the elastic properties also play an important role in how cracks propagate. For example, macroscopic models require the effective modulus of elasticity of the composite be known to model the propagation of bridged cracks [2], while micromechanical models of crack propagation require knowledge of the fiber, matrix and interface elastic properties [3].

The effort needed to characterize the thermo-mechanical response of composites and the amount of experimental data required can be sizable. Thus in parallel, it is desirable to formulate a micromechanical model. The essential quantities sought from such a model are the effective moduli, or a constitutive model relating the microstructural parameters of fiber, matrix, and interface to the macroscopic mechanical behavior of composites. Establishing such a model allows: (1) optimization of material behavior by tailoring the types and forms of the constituent components, and (2) to predict the thermo-mechanical response of the composite made of such materials. An example would be a simple rule of mixtures model that predicts the elastic properties of a composite material by taking the weighted means of the matrix and fiber elastic properties.

The purpose of this study is to establish a phenomenological micromechanical model and establish its range of validity for W_f/W composite materials being developed for fusion applications. To date, the macroscopic mechanical properties of such W_f/W composites have been characterized by destructive (3 point bending) [4], or non-destructive (laser ultrasonics) [5] testing. In this work, we test whether the rules of mixtures holds true for W_f/W composite materials as a function of fiber volume fraction. We experimentally measure the micro- and macro- scale elastic properties by nano-indentation and laser ultrasonic method, respectively.

2. Experiments

2.1. W_f/W composite samples

Short-fiber W_f/W samples manufactured by spark plasma sintering (SPS) process were used. In this process, W powder with a grain size of 5 μm and W-fibers with a length of 2.4 mm and diameter of 0.24 mm were mixed and sintered. Due to the mixing, the fibers were distributed homogeneously in random orientations leading to isotropic material behavior [4]. Different materials with varying fiber volume fraction

* Corresponding author.
E-mail address: heunlee@eei.eng.osaka-u.ac.jp (H.T. Lee).

https://doi.org/10.1016/j.nme.2019.03.001
Received 14 August 2018; Received in revised form 26 February 2019; Accepted 1 March 2019
Available online 08 March 2019

Table 1
Summary of W_f/W sample properties, wave velocities, and modulus determined by laser ultrasonic and nano-indentation methods.

W_f/W samples			Laser ultrasonic method						Nano-indentation method	
Fiber volume fraction (%)	Mean Density (kg/m^3)	Mean Thickness (mm)	C_L (m/s)	C_S (m/s)	Shear Modulus, μ (GPa)	Lame's constant, λ (GPa)	Poisson ratio, ν	Bulk modulus, K (GPa)	Young's modulus, E (GPa)	Avg. Young's modulus (Matrix) (GPa)	Avg. Young's modulus (Fiber) (GPa)
20	18,014 ± 27	3.78 ± 0.002	4800 ± 19	2656 ± 37	127 ± 3	161 ± 7	0.279 ± 0.008	246 ± 6	325 ± 9	329 ± 18	444 ± 4
40	18,010 ± 6	4.77 ± 0.004	4983 ± 10	2740 ± 23	136 ± 2	168 ± 4	0.276 ± 0.005	258 ± 3	347 ± 6	308 ± 15	397 ± 8
50	18,116 ± 4	4.54 ± 0.002	4902 ± 29	2734 ± 20	135 ± 1	165 ± 6	0.274 ± 0.005	255 ± 4	345 ± 4	322 ± 25	440 ± 7
60	18,209 ± 12	3.96 ± 0.001	4975 ± 90	2709 ± 41	134 ± 3	183 ± 17	0.289 ± 0.011	272 ± 12	337 ± 8	310 ± 9	438 ± 8

were prepared (20, 40, 50 and 60%). The samples density ranges from 93–94% of the theoretical density, as determined using the Archimedes method (see Table 1). Further details of the synthesis and the subsequent characterization can be found in Ref. [4]. The sample dimensions are shown in Fig. 1(a). One side of the sample was mechanically polished to allow nano-indentation and laser ultrasonic measurements.

2.2. Laser ultrasonic method

Laser ultrasonics is a non-contact and non-destructive technique to generate and detect elastic waves in materials [6]. The method can be used to identify surface cracks, measure changes in thickness, or detect changes in materials' mechanical properties. A pulsed laser generates elastic waves, which is detected using a second laser coupled to an interferometer. The wave velocity in a solid medium is closely related to the elastic properties of the propagating medium. There are two primary modes of ultrasound propagating inside a bulk material; longitudinal (L-) and shear (S-) waves. The method measures the averaged integrated property along the wave transport path [6].

A simplified schematic of the experimental setup is shown in Fig. 1(b). It consists of a Q-switched Nd:YAG laser beam to generate stress waves in materials and a Vibrometer to measure the stress waves. A sample is placed between the two laser beams on a 5 axes manual stage, which allows for XYZ translation as well as polar and tilt rotational movements. A conventional pulse-echo setup is used where the two lasers are coincident on the same axis (i.e. epicentral configuration). The Nd:YAG laser source (Spectra Physics Quanta-Ray INDI-40) generates a ~10 ns pulsed laser beam at a wavelength of 1064 nm. A beam splitter is used to divert a portion of the laser pulse to a photodiode, which provided a zero-time trigger for the oscilloscope. The maximum energy was 0.45 J, which was reduced to 10 ~ 20 mJ and focused to 0.1 ~ 1 mm radius spot at the sample surface. This corresponds to energy density on the specimen of 0.003–0.6 MJ/cm^2, which resulted in thermoelastic expansion or ablation, respectively. The Vibrometer consists of a focusable 632 nm laser sensor head (Polytec OFV-505) coupled to a controller (OFV-2570). The Vibrometer is capable of measuring surface displacements and velocities up to ± 75 nm and 3 m/s, respectively. The displacement and velocity information is recovered from the phase and frequency modulation of the Doppler shift, respectively. The controller has a bandwidth up to 24 MHz. The output of the controller is received by an oscilloscope (Tektronix MD4034-3) with bandwidth up to 350 MHz. Typically an average of 16 shots is measured to increase the signal to noise ratio. Using the primary and echo pulses, the longitudinal (L-) and shear (S-) wave velocities were determined using cross-correlation analysis [7]. All experiments were performed in a vacuum system at a pressure of 1.33×10^{-5} Pa. More details of the experimental setup can be found in Ref. [5].

2.3. Nano-indentation method

Nano-indentation micro-hardness was measured using Agilent Technologies, Inc. Model Nano Indentor G200 with a Berkovich type indentation tip. The continuous stiffness measurements (CSM) were carried out with nm oscillation to determine hardness and stiffness as a function of indentation depth. The software used the measured stiffness to calculate the reduced modulus, which was then converted to Young's modulus using standard relations. Here, the input required was the Poisson's ratio, which was calculated from the measured longitudinal and shear wave velocities (see Section 3.1, Eq. (1)). Measurements were taken at different locations within the fiber or matrix regions with about 100 μm separation to avoid the effect of adjacent measurements. Fig. 2(a) shows a representative SEM image of a W_f/W sample surface probed by nano-indentation. The different regions of the fiber and matrix regions can be clearly seen. Also, the characteristic shape of the Berkovich type indentation tip is also visible at the measured locations. Fig. 2(b) shows a typical depth profile of the modulus for 60% fiber

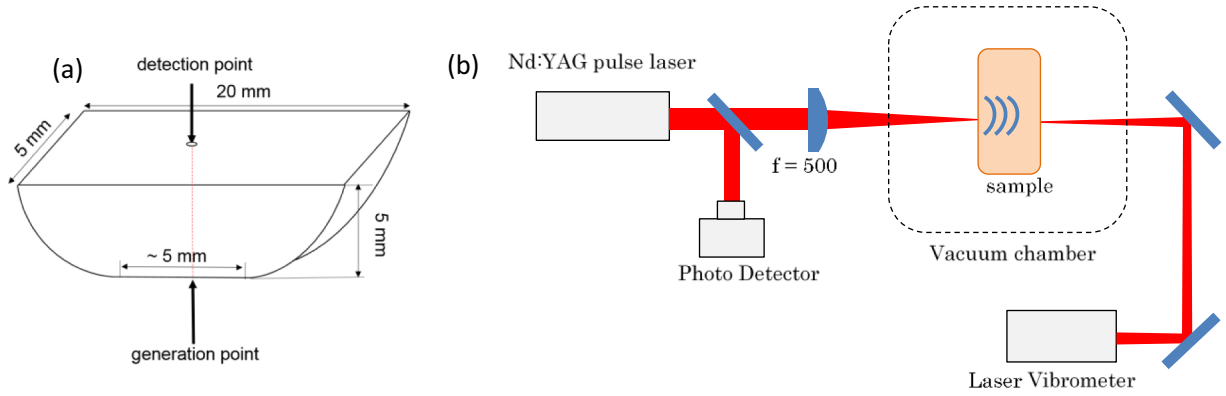

Fig. 1. (a) Dimensions of the samples used in experiments. The top surface was mechanically polished. The arrows indicate the position of the Vibrometer (detection point) and Nd:YAG lasers (generation point). (b) Schematic diagram of laser ultrasonic experimental setup. The measurement consists of a pulsed Nd:YAG laser to generate stress waves in materials, and a Vibrometer to measure the surface displacement and velocity. An epicentral configuration is shown where the two laser beams are aligned to the same axis.

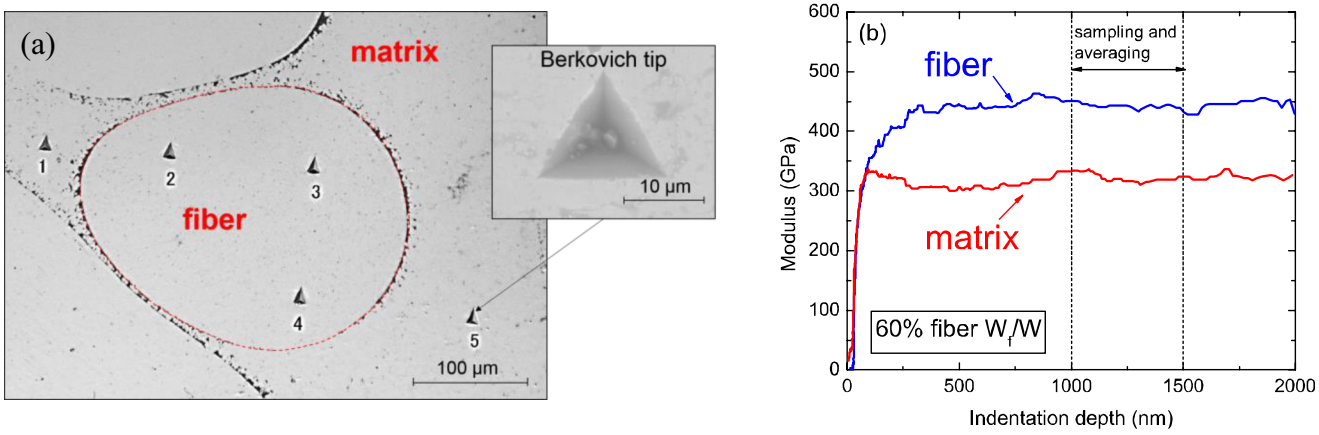

Fig. 2. (a) Representative SEM image of a W_f/W sample surface probed by nano-indentation. The different regions of the fiber and matrix regions can be clearly seen. Also, the characteristic shape of the Berkovich type indentation tip is also visible at the measured locations numbered 1–5. (b) Representative depth profile of the modulus for a 60% fiber volume fraction sample. To avoid surface effects, the modulus values in the range 1000–1500 nm were averaged.

volume fraction sample. It is clear that the fiber is stiffer than the matrix. To avoid surface effects, the modulus values in the range 1000–1500 nm were averaged.

3. Results and discussion

3.1. Wave velocities and modulus (macro-scale)

In Fig. 3, the L- and S- wave velocities are plotted for samples with different fiber volume fraction. The error bar spans the range of variation in wave velocities for ten different measurement locations. It is clear that the wave velocities do not scale monotonically with increasing fiber volume fraction. Also plotted are values for reference polycrystalline W (Ref-W), and pure-W samples manufactured using the SPS technique at two different sintering temperatures [5]. The dotted line indicates the best fit to all the data with the intercept fixed at zero. This line represents the ratio of wave velocities C_S/C_L and the slope is equal to 0.55. Poisson's ratio, ν, is expressed as a function of the wave velocities as follows:

$$\nu = \frac{1 - 2(C_S/C_L)^2}{2\{1 - (C_S/C_L)^2\}} \quad (1)$$

Using Eq. (1), $C_S/C_L = 0.55$ corresponds to a Poisson's ratio of 0.28, which is in excellent agreement with pure W (0.27–0.29) [8]. In addition, the shear modulus, μ is given by:

$$\mu = \rho C_S^2 \quad (2)$$

where ρ, is the density. Homogeneous isotropic elastic materials have their elastic properties uniquely determined by any two moduli. Thus, knowledge of Poisson's ratio and the shear modulus using Eqs. (1) and (2) allows any of the other elastic moduli to be calculated if the density, ρ, is known. As a first approximation, we treat the W_f/W samples as isotropic and homogeneous at the macro level. Table 1 summarizes the calculated values of the elastic moduli based on wave velocities measured by laser ultrasonic method (Poisson's ratio, shear modulus, Lame's constant, bulk modulus, and Young's modulus).

In Fig. 4, bulk and Young's modulus are plotted as a function of fiber volume fraction. The dotted lines are meant to guide the eye only. Note that laser ultrasonic measurement probes the average property along the wave transport path. It can be seen that the bulk modulus tends to increase monotonically with increasing fiber volume fraction. This is attributed to the fact that the sample density increases monotonically with increasing fiber volume fraction. In contrast, Young's modulus does not increase monotonically with increasing fiber volume fraction, but rather peaks between 40 and 50% fiber volume fractions. This indicates that despite an increase in density, the material is less stiff at 60% fiber volume fraction. The physical reason for the reduction in stiffness is not yet clear.

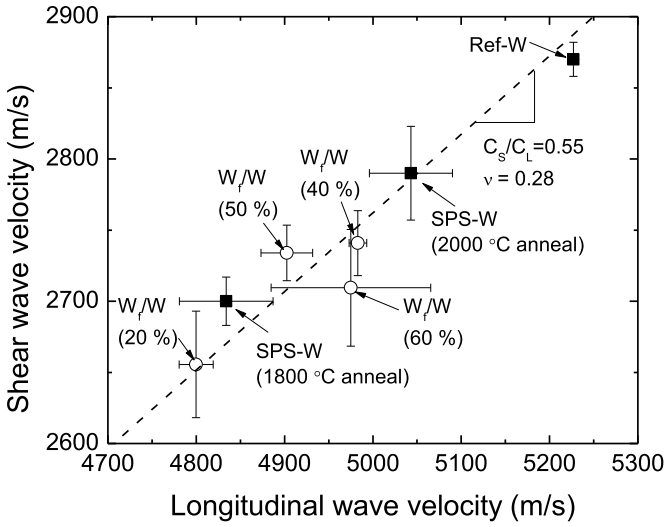

Fig. 3. Plot of shear vs. longitudinal wave velocities for W_f/W samples with different fiber volume fraction. Also plotted are values for reference polycrystalline W (Ref-W) manufactured by ALMT corp, and pure-W samples manufactured using the SPS technique at two different sintering temperatures [5]. The dashed line indicates the best fit to all the data with the intercept fixed at zero and corresponds to a Poisson's ratio of 0.28. The error bar for Ref-W indicates measurement and analysis error. The error bar for all other samples indicates the range of variation in velocities corresponding to different measurement locations.

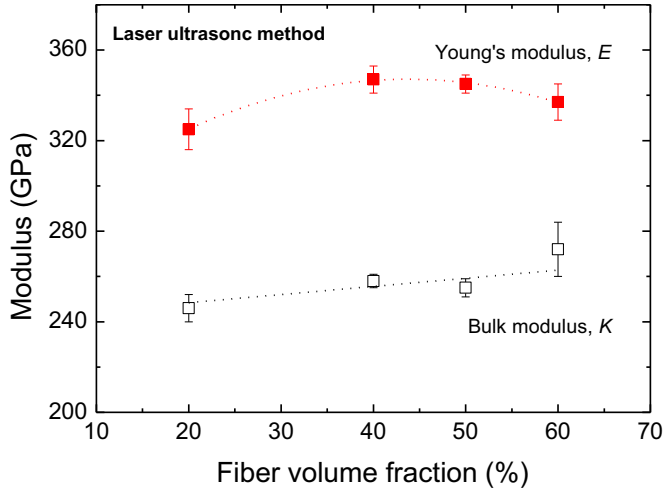

Fig. 4. Calculated values of bulk modulus, K, and Young's modulus, E, using the wave velocities determined from laser ultrasonic method. The dotted lines are meant to guide the eye only.

3.2. Modulus from nano-indentation (micro-scale)

In Fig. 5, the modulus determined from nano-indentation method is plotted as a function of fiber volume fraction for both fiber and matrix regions. The data plotted is the averaged value between 1000 – 1500 nm depths. The error bar indicates the standard deviation in the measured values over ten different measurement locations. In the case of the fiber, the data represents the averaged measurements along both the transverse and parallel orientations. The average value for the fiber (~440 GPa) is stiffer than the matrix (~310 GPa). The lower matrix values as well as its larger variation are thought to arise from effects of porosity. These values are higher and lower than the modulus of polycrystalline W (406 GPa) [5], respectively. The reason for the outlier data for the fiber at 40% fiber volume fraction is unknown. One possibility is that the sample surface is contaminated affecting the near surface characteristics of the fibers. The data is also summarized in Table 1.

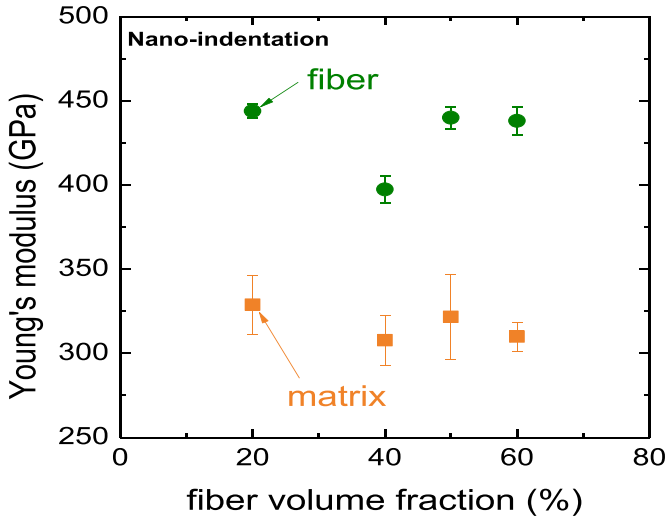

Fig. 5. The modulus determined from nano-indentation method is plotted as a function of fiber volume fraction for both fiber and matrix regions. The data plotted is the averaged value between 1000 – 1500 nm depths. The error bar spans the range of variation in modulus for ten different measurement locations. In the case of the fiber, the data represents the averaged measurements along both the transverse and parallel orientations.

3.3. Testing the rule of mixture for W_f/W samples

The rule of mixtures used to predict the elastic properties of a composite material takes the weighted means of the matrix and fiber properties as seen below:

$$E_{comp} = E_f V_f + E_m(1 - V_f) \quad (3)$$

where E_{comp}, E_f, E_m and V_f corresponds to the macroscopic bulk modulus, fiber modulus, matrix modulus, and fiber volume fraction, respectively. In this approximation, the length of the fiber is ignored, and the elastic property is considered parallel along the fiber orientation. To

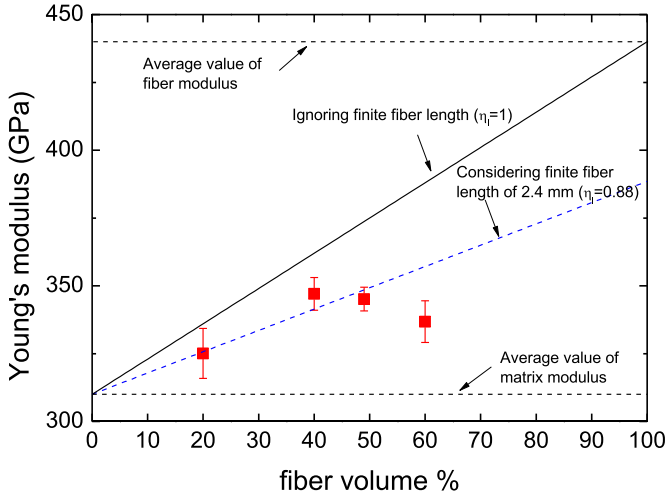

Fig. 6. Young's modulus of W_f/W samples as a function of fiber volume fraction probed by laser ultrasonic (solid red) method. Eqs. (3) and (4) are plotted as a function of fiber volume fraction in solid black and dashed blue lines, respectively. Here, the fiber (E_f = 440 GPa) and matrix (E_m = 310 GPa) modulus are taken to be the average values determined from nano-indentation method (see Fig. 5 or Section 3.2).

account for finite fiber length, a correction term η_l is added as seen below [9]:

$$E_{comp} = \eta_l E_f V_f + E_m(1 - V_f) \tag{4}$$

where η_l corresponds to a stiffness reduction ratio arising from finite fiber length, l. It is derived from analysis of how locally a state of uniform stress and strain in the matrix is perturbed by the transfer of load to the fibers. It is assumed that the lateral stiffness of the fibers is the same as that of the matrix, and the load in the direction of the length of the fiber is shared between the fiber and matrix. The mean load transferred between the fiber and matrix is then subject to geometrical constraints like the fiber length and is defined as follows [9]:

$$\eta_l = 1 - \left(\tanh\frac{1}{2}\beta l\right)\Big/(1/2\beta l) \tag{5}$$

$$\beta = \sqrt{\frac{2\mu_f}{E_f r_f^2 l \cdot n\left(\frac{R}{r_f}\right)}} \tag{6}$$

where r_f and μ_f corresponds to fiber radius and shear modulus. The fiber shear modulus was calculated using the expression $\mu_f = E_f/2(1+\nu)$ using the measured Young's modulus of the fiber and taking the Poisson's ratio of 0.28. 2R represents the distance between adjacent fibers and when fibers are homogeneously arranged is approximated by:

$$R = \frac{r_f}{2}\sqrt{\left(\frac{\pi}{V_f}\right)} \tag{7}$$

For W_f/W samples, the stiffness reduction ratio was calculated to be $\eta_l = 0.88$ (fiber length = 2.4 mm; diameter = 0.24 mm).

Eqs. (3) and (4) are plotted in Fig. 6 as a function of fiber volume fraction in solid black and dashed blue lines, respectively. Here, the fiber ($E_f = 440\ GPa$) and matrix ($E_m = 310\ GPa$) modulus are taken to be the average values determined from nano-indentation method (see Fig. 5 or Section 3.2). For comparison, the macroscopic averaged values determined by laser ultrasonics from Fig. 4 are also plotted (solid red symbols). One can see that the values determined from the rules of mixture agree within experimental error with macroscopic values measured using laser ultrasonics. Such comparison suggests that the simple rule of mixture is sufficiently accurate in predicting bulk elastic properties of W_f/W samples, but only up to 50% fiber volume fraction sample. The experimentally determined modulus does not monotonically increase with fiber volume fraction as predicted by Eq. (4). The reason for such discrepancy must lie in some other parameter that is not taken into account in the model, and will be the focus of future work.

4. Conclusion

The elastic properties of tungsten fiber-reinforced tungsten composites (W_f/W) were characterized on the micro- and macro- scale by combined nano-indentation and laser ultrasonic measurements respectively. Nano-indentation was used to measure the local micro-scale elastic modulus of fiber and matrix, separately. Laser ultrasonic method was used to measure the bulk macro-scale elastic modulus. The rules of mixture predicted a monotonic increase in elastic modulus with increasing fiber volume fraction. Experimentally, this was observed to be true only up to 50% fiber volume fraction. The reason for such discrepancy may be due to fiber-fiber interactions at higher fiber volume fraction but remains future work to clarify. For the present synthesis method, 40–50% fiber volume fraction leads to the highest Young's modulus at ~350 GPa.

Acknowledgments

This work was partially supported by JSPS Grant-in-Aid for Young Scientists (B) no. 26820397 and by the ZE Research Program, IAE (ZE29A-16). Travel support by Kansai Research Foundation (2018F004) is gratefully acknowledged.

References

[1] J.W. Coenen, et al., Fusion Eng. Design 124 (2017) 964.
[2] B.N. Cox, D.B. Marshall, Acta Metall. Mater. 39 (1991) 579.
[3] V.C. Li, et al., J. Mech. Phys. Solids 39 (1991) 607.
[4] Y. Mao, et al., Phys. Scr. T 170 (2017) 014005.
[5] H.T. Lee, et al., Phys. Scr. T 170 (2017) 014024.
[6] C.B. Scruby, L.E. Drain, Laser Ultrasonics: Techniques and Applications, IOP publishing, 1990.
[7] J.D. Aussel, J.P. Monchalin, Ultrasonics 27 (1989) 165.
[8] E. Lassner, W.D. Schubert, Tungsten: Properties, Chemistry, Technology of the Element, Alloys, Springer publishing, 1999.
[9] H.L. Cox, Brit. J. Appl. Phys. 3 (1952) 72.